

*Citation for published version:*

Pérez-Mendoza, M, González, J, Ferreiro-Rangel, CA, Lozinska, MM, Fairén-Jiménez, D, Düren, T, Wright, PA & Seaton, NA 2014, 'Pore-network connectivity and molecular sieving of normal and isoalkanes in the mesoporous silica SBA-2', *Journal of Physical Chemistry C*, vol. 118, no. 19, pp. 10183-10190.  
<https://doi.org/10.1021/jp502390p>

*DOI:*

[10.1021/jp502390p](https://doi.org/10.1021/jp502390p)

*Publication date:*

2014

*Document Version*

Peer reviewed version

[Link to publication](#)

This document is the Accepted Manuscript version of a published work that appeared in final form in The Journal of Physical Chemistry C, copyright (C) American Chemical Society after peer review and technical editing by the publisher. To access the final edited and published work see <http://doi.org/10.1021/jp502390p>

**University of Bath**

## **Alternative formats**

If you require this document in an alternative format, please contact:  
[openaccess@bath.ac.uk](mailto:openaccess@bath.ac.uk)

### **General rights**

Copyright and moral rights for the publications made accessible in the public portal are retained by the authors and/or other copyright owners and it is a condition of accessing publications that users recognise and abide by the legal requirements associated with these rights.

### **Take down policy**

If you believe that this document breaches copyright please contact us providing details, and we will remove access to the work immediately and investigate your claim.

This document is confidential and is proprietary to the American Chemical Society and its authors. Do not copy or disclose without written permission. If you have received this item in error, notify the sender and delete all copies.

**Pore-Network Connectivity and Molecular Sieving of Normal and Iso-Alkanes in the Mesoporous Silica SBA-2**

Journal:	<i>The Journal of Physical Chemistry</i>
Manuscript ID:	jp-2014-02390p
Manuscript Type:	Article
Date Submitted by the Author:	09-Mar-2014
Complete List of Authors:	Perez-Mendoza, Manuel; University of Granada, Departamento de Quimica Inorganica González, Jorge; Escuela de ciencias químicas, Universidad de Colima Ferreiro-Rangel, Carlos; University of Edinburgh, School of Engineering Lozinska, Magdalena; University of St Andrews, Chemistry Fairen-Jimenez, David; University of Cambridge, Dept. of Chemical Engineering & Biotechnology Düren, Tina; University of Edinburgh, School of Engineering Wright, Paul; University of St. Andrews, Chemistry Seaton, Nigel; University of Edinburgh,

SCHOLARONE™  
Manuscripts

1  
2  
3  
4  
5  
6  
7  
8  
9  
10  
11  
12  
13  
14  
15  
16  
17  
18  
19  
20  
21  
22  
23  
24  
25  
26  
27  
28  
29  
30  
31  
32  
33  
34  
35  
36  
37  
38  
39  
40  
41  
42  
43  
44  
45  
46  
47  
48  
49  
50  
51  
52  
53  
54  
55  
56  
57  
58  
59  
60

# Pore-Network Connectivity and Molecular Sieving of Normal and Iso-Alkanes in the Mesoporous Silica SBA-2

*Manuel Pérez-Mendoza<sup>\*,†</sup>, Jorge González<sup>‡,§</sup>, Carlos A. Ferreiro-Rangel<sup>§</sup>, Magdalena M.*

*Lozinska<sup>‡</sup>, David Fairén-Jiménez<sup>§,¶</sup>, Tina Düren<sup>§</sup>, Paul A. Wright<sup>‡</sup>, Nigel A. Seaton<sup>§,\*</sup>*

<sup>†</sup> Departamento de Química Inorgánica, Facultad de Ciencias, Universidad de Granada, 18071  
Granada, Spain.

<sup>§</sup> Institute for Materials and Processes, School of Engineering, The University of Edinburgh,  
King's Buildings, Edinburgh, EH9 3JL, UK, UK.

<sup>‡</sup> EaStCHEM School of Chemistry, University of St Andrews, North Haugh, St Andrews, Fife,  
KY16 9ST.

<sup>§</sup> Facultad de Ciencias Químicas, Universidad de Colima, Colima, 28040, México

KEYWORDS: SBA-2 structure, normal and iso-alkane separation, pore-network connectivity,  
molecular sieving, percolation, molecular simulation, adsorbent design.

1  
2  
3 ABSTRACT: We have studied the adsorption of n-butane and iso-butane in the mesoporous  
4 silica SBA-2. Our work has two purposes: (i) to better understand the structure of the material,  
5 and in particular the impact of calcination on the evolution of the pore network; and (ii) to  
6 investigate our ability to tune the structure of SBA-2 to separate normal and iso-alkanes by  
7 molecular sieving. By a combination of experimental adsorption measurements, molecular  
8 simulation, and percolation analysis, we determined the evolution of the sizes of the pores and  
9 the connectivity of the pore network as the calcination temperature increases. For a certain range  
10 of calcination temperatures, the pore network drops below its percolation threshold for iso-  
11 butane, while allowing the percolation of n-butane, giving an extremely high selectivity for n-  
12 butane over iso-butane. This suggests that tuning the window size of SBA-2 and other structured  
13 mesoporous materials of this general type has the potential to generate optimized adsorbents for  
14 particular applications.  
15  
16  
17  
18  
19  
20  
21  
22  
23  
24  
25  
26  
27  
28  
29  
30  
31

## 32 33 1. INTRODUCTION

34  
35 Since their discovery in the early nineties<sup>1-2</sup>, periodic mesoporous silicas (PMSs) have become  
36 one of the most versatile families of materials with applications in, for example, gas separation,  
37 adsorption, controlled drug release, shape-selective catalytic processes and sensing<sup>3-5</sup>. The way  
38 they are synthesized, using a precursor solution with a silica source and a liquid-crystal phase  
39 formed by a surfactant which serves as a template for the porous material, followed by the  
40 calcination of the resultant silica network, is the origin of their versatility<sup>1-2,6</sup>. Firstly, the  
41 template generates a well-defined long-range order in the structure, whilst at an atomic level the  
42 material is non-crystalline. The use of different precursor solutions and reaction conditions leads  
43 to different structures and PMSs exist with mono-, bi-, or tri-dimensional pore networks and with  
44 a wide range of pore sizes<sup>7-9</sup>. The pore size and connectivity of the network affects the  
45  
46  
47  
48  
49  
50  
51  
52  
53  
54  
55  
56  
57  
58  
59  
60

1  
2  
3 equilibrium and dynamics of molecular processes occurring within the pore space such as the  
4  
5 adsorption and diffusion of gases. Secondly, the surface chemistry of the pores can be modified  
6  
7  
8 by lining with organic groups and metals either by in situ co-condensation or by post-synthesis  
9  
10 grafting<sup>10-11</sup>, changing for example the hydrophilicity and acidity of the materials, with all the  
11  
12 implications this has for their possible uses in selective adsorption and catalysis.  
13  
14

15 SBA-2 is a PMS with a three-dimensional pore network<sup>12-13</sup>. One of the distinctive features of  
16  
17 SBA-2 is that the topology of the network is formed by spherical cavities arranged in either  
18  
19 hexagonal close-packed (hcp) or cubic close-packed (ccp) networks, with diameters in the  
20  
21 mesopore size-range that are interconnected by smaller, cylindrical channels, with sizes in the  
22  
23 micropore size-range<sup>12-14</sup>. (The ccp material is strictly designated STAC-1, but in this paper we  
24  
25 use for convenience the term SBA-2 to refer to both materials. In practice, samples typically  
26  
27 contain materials with both structures, intergrown, although recently both pure ccp and pure  
28  
29 hexagonal close packed structures have been prepared using a costructure directing agent and  
30  
31 gemini surfactant under closely controlled conditions<sup>15-16</sup>). Thus, the pore structure combines the  
32  
33 large volume associated with the cage-like pores with the selectivity with respect to molecular  
34  
35 size and shape of the narrow microporous channels. This combination is attractive for  
36  
37 applications such as adsorptive separations and shape-selective catalysis.  
38  
39  
40  
41  
42

43 The channels appear to originate in the close proximity of the spherical micelles during the  
44  
45 synthesis process, leading to a concentration of water molecules at the interface, and a  
46  
47 corresponding tendency for the silica condensation in this region to be relatively slight<sup>17</sup>. We  
48  
49 have also suggested that the channels might be further developed when the synthesized material  
50  
51 is calcined to remove the surfactant<sup>18</sup>. It is thus unlikely that the cages will be connected  
52  
53 following a completely regular pattern and that all the channels will have the same size. It is  
54  
55  
56  
57  
58  
59  
60

1  
2  
3 more likely that the calcination process will have an important effect on how these channels are  
4 formed and, hence, on the connectivity of the porous network – that is, on the number and size of  
5 the channels connecting the cavities. As the connectivity has a direct effect on the accessibility of  
6 the channels connecting the cavities. As the connectivity has a direct effect on the accessibility of  
7 adsorptives to the pores, this will condition the performance of SBA-2 material as an adsorbent  
8 or catalyst support. Therefore, establishing and controlling the relationship between preparation  
9 and performance is crucial from the materials design point of view.

10  
11  
12  
13  
14  
15  
16  
17 In a previous communication<sup>14</sup>, we showed that a model based on a pore size distribution  
18 (PSD) of cylinders (representing the interconnecting channels) and spheres (representing the  
19 spherical cavities) is able to describe and accurately predict the adsorption of methane and ethane  
20 on SBA-2 using the grand canonical Monte Carlo (GCMC) simulation method. In a subsequent  
21 paper<sup>18</sup>, we showed that percolation theory, together with the PSD analysis, can be used to  
22 understand the accessibility of the pore network to molecules of different sizes and shapes, and  
23 hence to evaluate the connectivity of the network. The results indicated a much lower effective  
24 coordination number for the cavities than expected from the geometric structure of the system.  
25 The network was sufficiently well connected that it was above the percolation threshold for both  
26 species studied, nitrogen and ethane. That is, both species could gain access to all macroscopic  
27 regions of the material, though not necessary to every individual cavity. The effective  
28 coordination numbers experienced by the two species were very different, however: 4.9 for  
29 nitrogen and 1.8 for ethane. (The value for ethane is just above the percolation threshold for the  
30 SBA-2 network, which percolates when the effective coordination number is 1.44<sup>19</sup>).

31  
32  
33  
34  
35  
36  
37  
38  
39  
40  
41  
42  
43  
44  
45  
46  
47  
48  
49  
50  
51  
52  
53  
54  
55  
56  
57  
58  
59  
60  
The purpose of the present work is to improve our understanding of the pore structure of SBA-  
2 by applying the adsorption-percolation analysis to larger adsorptives with different shapes, n-  
butane (C4) and iso-butane (isoC4), and to use this analysis to understand the relationship

1  
2  
3 between the temperature of calcination and the pore structure. This is important for two reasons.  
4  
5 Firstly, by using larger molecules than in our earlier study<sup>18</sup> we gain further insights into the  
6  
7 effect of the manufacturing process on the pore structure of SBA-2. Secondly, we are interested  
8  
9 in the potential of SBA-2 for shape-selective adsorption in applications in which a high  
10  
11 adsorption capacity is important. The C<sub>4</sub>/isoC<sub>4</sub> system is an example of an important class of  
12  
13 industrial processes in which normal and iso-alkanes are separated.  
14  
15  
16  
17  
18  
19

## 20 2. EXPERIMENTAL SECTION

21  
22 The SBA-2 samples were prepared at room temperature and alkaline pH using a gemini  
23  
24 quaternary ammonium surfactant as template. A complete description of the preparation  
25  
26 methodology has been previously reported<sup>12</sup>. Different batches calcined at 700, 800 and 900 °C  
27  
28 were prepared to study the influence of calcination temperature in the structure. A solvent-  
29  
30 extracted sample (with no calcination) was also prepared. Further samples calcined at 550 and  
31  
32 820 °C were prepared for the study of mixture adsorption.  
33  
34  
35

36  
37 Powder X-ray diffraction patterns were collected in transmission mode in the form of powder  
38  
39 supported in 0.7 mm quartz glass capillaries. Measurements were made at ambient temperature  
40  
41 using monochromated Cu K<sub>α1</sub> radiation,  $\lambda = 1.54056 \text{ \AA}$ , on a STOE Stadi/p diffractometer.  
42  
43

44  
45 Transmission electron microscopy (TEM) micrographs were taken using a JEOL-JEM 2011  
46  
47 electron microscope equipped with a CCD Gatan digital camera operating at 200 keV. Samples  
48  
49 were ground before being dispersed in acetone then deposited onto a holey carbon film,  
50  
51 supported on a Cu grid.  
52

53  
54 The adsorption of nitrogen at 77 K and C<sub>4</sub> and isoC<sub>4</sub> at 268 K was measured from 0-1 bar  
55  
56 using a Hiden IGA automated gravimetric analyzer. Typically 10-25 mg of sample were used in  
57  
58  
59  
60

1  
2  
3 the determination of each isotherm. Samples were degassed at 383 K for 3h under vacuum and  
4  
5 cooled to room temperature before the dry mass was set. For nitrogen the sample chamber was  
6  
7 immersed in liquid nitrogen, whereas for the butanes the temperature of the sample chamber was  
8  
9 regulated by a Grants Optima GR150 thermostatic recirculating water bath.  
10  
11

12 Mixture adsorption experiments were carried out on a bench-scale open-flow  
13  
14 adsorption/desorption system. The system has been described previously<sup>20</sup>. In essence, a mixture  
15  
16 of a constant composition is allowed to flow past the sample until the outlet composition of the  
17  
18 gas reaches steady-state, at which point adsorption equilibrium is judged to have been attained.  
19  
20 The adsorbed phase is then desorbed by heating to 423 K, and collected in a container cooled to  
21  
22 77 K. The amount and composition of the adsorbate is then measured. In these experiments, a  
23  
24 1:1 C4/isoC4 gas mixture was allowed to flow past the sample at 268 K and 0.8 bar.  
25  
26  
27  
28  
29  
30  
31

### 32 3. ADSORPTION-PERCOLATION ANALYSIS

33

34 The essence of our approach is to treat separately two aspects of adsorption on this material,  
35  
36 each of which relates to a different length scale: the local adsorption equilibrium within  
37  
38 individual pores; and the effect that the pore network has on the accessibility of those pores to  
39  
40 different adsorptive species. As in our previous work<sup>14,18</sup>, the channels and cavities in SBA-2 are  
41  
42 represented by, respectively, cylindrical and spherical pores, with the pores having a regular,  
43  
44 atomistic surface. The adsorption of a particular species in a particular pore (either a cavity or a  
45  
46 channel, with a specified diameter) is modeled using grand canonical Monte Carlo (GCMC)  
47  
48 simulation, which generates a local adsorption isotherm, i.e. the equilibrium amount adsorbed as  
49  
50 a function of pressure. At this level of the model, the pores are considered to be independent of  
51  
52  
53  
54  
55  
56  
57  
58  
59  
60



1  
2  
3 each other; that is, the fact that in reality the pores are connected together in a network is  
4  
5 ignored. A complete description of the GCMC method used can be found in our earlier paper<sup>14</sup>.  
6  
7

8 It should be noted that a more rigorous treatment of adsorption on SBA-2 would treat the pore  
9  
10 network in an integral way, that is, without separately defining cavities and channels as “building  
11  
12 blocks” of the network. We have recently published an account of this approach, using a kinetic  
13  
14 Monte Carlo (kMC) method to simulate the synthesis of SBA-2 (and the closely related material  
15  
16 STAC-1)<sup>17</sup>. Using this approach, the connections between the cavities arise naturally from the  
17  
18 simulation. Both the individual cavities and the connections between them are, naturally, rather  
19  
20 irregular, whilst in a statistical sense the cavities remain spherical and their connections have an  
21  
22 approximately circular cross-section (though their cross-sectional area varies along their axis).  
23  
24  
25

26 The model materials generated by kMC simulation - which we take to be a good representation  
27  
28 of the real materials - thus support the use of spherical cavities in the present, simpler model.  
29  
30

31 The representation of the connections generated by kMC simulation as cylinders in the present  
32  
33 model is less exact, but the present approach captures the essence of the connections as short,  
34  
35 narrow elements with small but finite adsorption capacity. Whilst kMC simulation gives  
36  
37 powerful insights into the synthesis and properties of the real materials, the computational  
38  
39 demands of that approach are far too great for that method to be used for the extensive  
40  
41 adsorption-percolation analysis reported here.  
42  
43  
44

45 In our simulations, nitrogen was modeled as a two-site Lennard-Jones (LJ) molecule with a  
46  
47 quadrupole, following Kjems and Dolling<sup>21</sup>. C4 and isoC4 were modeled as four-site molecules,  
48  
49 with the CH<sub>3</sub>, CH<sub>2</sub> or CH groups represented by individual LJ sites. The potential parameters are  
50  
51 given in Table 1. The silicon atoms are neglected, with their small contribution to the adsorption  
52  
53 potential<sup>22</sup> implicitly included in the potential parameters of the oxygen atoms.  
54  
55  
56  
57  
58  
59  
60

The impact of the pore network on the adsorption - and in particular the effect of constrictions in the network on the accessibility of the pores to different adsorptive species - is modeled using percolation theory. To transform the problem of adsorption on SBA-2 into percolation terms we note that the accessibility of the network is controlled by the channels (“bonds”, in the language of percolation), as the cavities (“sites”, in percolation terms) are much larger than both the adsorptive species studied. The channels are of a comparable size to the adsorptive species, so that some permit the passage of both butane isomers (C4 and isoC4), some permit only the passage of the less bulky species (C4) and some permit the passage of neither species. Indeed, our earlier work<sup>18</sup> showed that some channels in SBA-2 are too small even to permit the passage of nitrogen, and that some of the channels that would correspond to a fully coordinated network might even be completely absent.

**Table 1:** Potential parameters for the fluids and SBA-2.

molecule	$\epsilon/k_B, K$	$\sigma, \text{\AA}$	quad. Moment, $C \cdot m^2$	bond length, $\text{\AA}$
$N_2$ (2 CLJ) <sup>21</sup>	33.4	3.383	-3.712	0.923
$C_4(CH_3)^{23}$	88.1	3.905	-	1.53
$C_4(CH_2)^{23}$	59.4	3.905	-	1.53
iso $C_4(CH_3)^{23}$	80.5	3.910	-	1.53
iso $C_4(CH)^{23}$	40.3	3.850	-	1.53
O	185.0	2.708	-	

Adsorption on SBA-2 is an example of percolation on a regular lattice. In the simplest form of lattice percolation, the individual elements are either the sites or the bonds. In “site percolation”, the network percolates if sufficient sites are occupied so that a connected network of sites spans the network. One then quantifies, for example, the proportion of the sites that are in the

1  
2  
3 percolating cluster of sites – the “accessibility” of the sites. In “bond percolation”, the network  
4  
5  
6 percolates if sufficient bonds are occupied, and one calculates the accessibility of the bonds.  
7  
8 Adsorption in SBA-2 corresponds to a more complex percolation problem in which both sites  
9  
10 and bonds must be considered. The bonds determine the accessibility of the network, while both  
11  
12 the sites and the bonds contribute to adsorption. In percolation terms, a site or bond is defined to  
13  
14 be “occupied” if it is large enough to accommodate the species of interest, so that a percolating  
15  
16 cluster of sites and bonds would allow adsorption of that species. In the study of the adsorption  
17  
18 of nitrogen, C4 and isoC4 on SBA-2, all the sites are occupied as they are larger than all these  
19  
20 species; the site occupation probability,  $p^s = 1$ . In contrast, only some of the bonds are occupied,  
21  
22 i.e. are large enough to allow the passage of the species; the bond occupation probability,  $p^b < 1$ .  
23  
24 Thus, adsorption in the channels corresponds to bond percolation, while adsorption in the  
25  
26 cavities corresponds to what is sometimes termed “site percolation in the bond problem”<sup>19</sup>. In the  
27  
28 latter case, the network elements of fundamental interest are the sites, while their accessibility is  
29  
30 controlled by the bonds; in adsorption terms, adsorption in the cavities is controlled by passage  
31  
32 of the adsorptive species through the channels.  
33  
34  
35  
36  
37  
38

39 The network variable that controls the accessibility of both the sites and the bonds (and hence  
40  
41 the overall adsorption) is thus the bond occupation probability,  $p^b$ . This has a different value,  
42  
43  $p^{b,i}$ , for each species,  $i$ .  $p^{b,i}$  is related to the mean number of channels per cavity that are large  
44  
45 enough to accommodate that species (the “effective” coordination number),  $z^i$ , by

$$z^i = Zp^{b,i} \quad (1)$$

46  
47  
48 where  $Z$  is the coordination number of the network;  $Z = 12$  for both hcp and ccp networks. The  
49  
50 percolation behavior of a network with  $Z = 12$  has been computed by Yanuka<sup>19</sup> for both bond  
51  
52 percolation and “site percolation in the bond problem”. [Yanuka studied only the ccp network.  
53  
54  
55  
56  
57  
58  
59  
60

1  
2  
3 However, as the percolation properties of a network depend mainly on the dimensionality and  
4 coordination number, and only to a small extent on other aspects of the topology<sup>24</sup>, Yanuka's  
5 results are applicable to both the ccp and hcp forms of the SBA-2 network].  
6  
7

8  
9  
10 The first step in the connectivity analysis<sup>18</sup> is to determine the accessibility of the sites to each  
11 species. This is done by using the simulated adsorption isotherms to obtain the pore size  
12 distribution (PSD) of the cavities. By using nitrogen, C4 and isoC4 in turn, we obtain three  
13 different PSDs, each describing the portion of the pore network that is probed by that species.  
14 IsoC4 is more bulky than C4, which in turn is more bulky than nitrogen, so the PSDs are  
15 expected to show peaks that diminish in magnitude in the order isoC4 > C4 > nitrogen.  
16  
17  
18  
19  
20  
21  
22  
23

24 We root the present analysis in information about the accessibility of the SBA-2 pore network  
25 from our earlier work<sup>18</sup>. In that work, the SBA-2 sample was prepared by post-synthesis  
26 calcination at 550 °C. The nitrogen adsorption isotherm of that material is almost identical to  
27 that of the solvent-extracted sample in the present work (reflecting the relatively mild effect of  
28 calcination at that relatively low temperature, Figure S1). We are thus able to use the bond  
29 occupation probability for nitrogen,  $p^{b,n} = 0.41$  (corresponding to  $z^n = 4.9$ ) from that study and  
30 apply it to the present solvent-extracted sample. Our adsorption-percolation analysis thus  
31 measures changes in the connectivity of the pore network of the various calcined samples, as  
32 experienced by different species, relative to the datum of nitrogen adsorption in the solvent-  
33 extracted sample. The fraction of cavities accessible to species  $i$ ,  $P^{s,i}$  is related to the PSD by:  
34  
35  
36  
37  
38  
39  
40  
41  
42  
43  
44  
45  
46  
47

$$48 \quad P^{s,i} = \frac{\int_0^\infty f^i(r) dr}{\int_0^\infty f^n(r) dr} \quad (2)$$

49 where  $f^i(r) = dN^i/dr$ :  $N^i$  is the number of pores, so that  $f^i(r)$  is the probability density function for  
50 the number of pores as a function of pore radius.  $f^n(r)$  is the “reference” distribution, measured  
51 using the adsorption of nitrogen on the solvent-extracted sample.  
52  
53  
54  
55  
56  
57  
58  
59  
60

1  
2  
3 The precise definition of the PSD used in eq (2) requires some discussion. The conventional  
4 definition of the PSD, and the form that is obtained directly from adsorption measurements, is  
5 the distribution of the pore volume, rather than the pore number, as a function of pore radius; for  
6 the spherical cavities considered here,  $dN^i/dr = 1/r^3 \cdot dV^i/dr$ . For a given material, the set of  
7 cavities explored by different adsorptive species differ in their connections to other pores, but not  
8 – in a statistical sense – in their size. The ratio of the numbers of pores accessible to different  
9 species is therefore the same as the ratio of the pore volumes accessible to different species. In  
10 such a case, eq (2) could identically be written in terms of  $dV^i/dr$  rather than  $dN^i/dr$ . Indeed, this  
11 approach was taken in our earlier paper<sup>18</sup>. However, when comparisons are being made between  
12 different materials – in our case, samples of SBA-2 calcined at different temperatures, or solvent-  
13 extracted – the relationship between accessible volume and accessible number of pores is  
14 different for different materials. The materials represented by the numerator and the denominator  
15 of eq (2) are different, so the fundamentally correct pore number distribution,  $dN^i/dr$ , must be  
16 used.

17  
18  
19  
20  
21  
22  
23  
24  
25  
26  
27  
28  
29  
30  
31  
32  
33  
34  
35  
36  
37  
38  
39  
40  
41  
42  
43  
44  
45  
46  
47  
48  
49  
50  
51  
52  
53  
54  
55  
56  
57  
58  
59  
60  
The PSD analysis was carried out by solving the adsorption integral equation using the  
numerical approach of Davies and Seaton<sup>25</sup>. This relates the overall adsorption, as measured in  
an experiment, to adsorption in individual pores, represented by molecular simulations of  
adsorption on model cylindrical and spherical model pores of different sizes.

Once  $P^{s,i}$  has been obtained, we use Yanuka's results for site percolation in the bond problem<sup>19</sup>  
(shown in Figure 1) in the cavities to obtain  $p^{b,i}$ , which in turn gives the effective coordination  
number for this species,  $z^i$ .

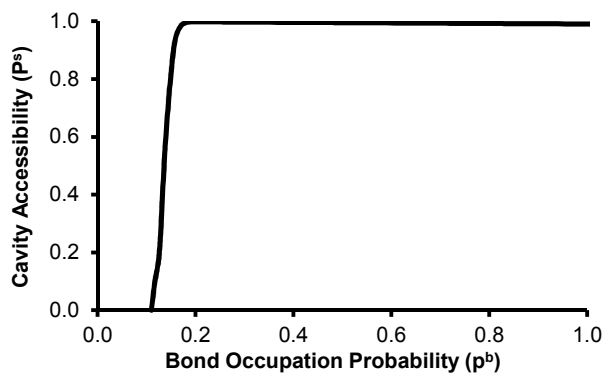


**Figure 1:** Yanuka's function for site percolation in the bond problem in fcc lattice<sup>19</sup>.

Thus, the problem of characterizing the connectivity of our SBA-2 network is reduced to the determination of the fraction of cavities accessible to the different adsorptive species under study, which in turn requires the determination of the PSD of the portion of the pore network that is probed by those species. In our work, the PSDs of the portions of the network accessible to nitrogen, butane and isobutane were obtained by analyzing the experimental adsorption isotherms of those species (at 77 K, for nitrogen, and 268 K for C4 and isoC4).

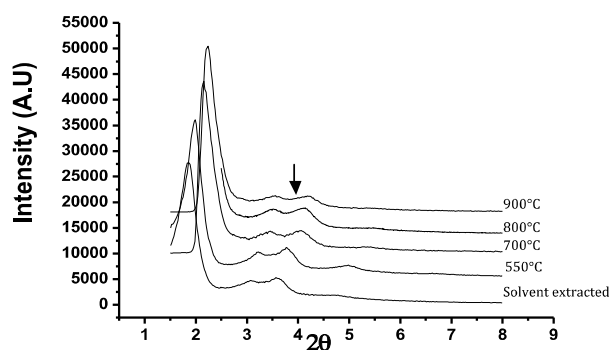
In summary, the steps in the adsorption-percolation analysis of each sample are as follows:

1. For each adsorptive, the PSD is obtained using nitrogen, C4 and isoC4.
2. The PSDs are integrated using Eq. (2) to obtain  $P^{s,i}$ .
3. The data of Figure 1 are used to obtain  $p^{b,i}$ .
4. The effective coordination number experienced by each species is obtained from Eq. (1).

#### 4. RESULTS AND DISCUSSION

XRD analysis of the samples calcined at different temperatures shows that the symmetry of the network is preserved through the calcination process even for the highest calcination temperature (Figure 2). High resolution transmission electron microscopy confirmed that the ordered close packed array of cages remained after each calcination<sup>26</sup>. Huo et al.<sup>27</sup> reported that silicate SBA-2

1  
2  
3 material was thermally stable up to 800 °C. It is clear from our XRD and TEM analysis that the  
4  
5 SBA-2 is actually stable up to 900 °C. Nevertheless, the diffraction maxima shift progressively to  
6  
7 higher angles with the increase in calcination temperature, indicating a systematic contraction of  
8  
9 the unit cell. TEM micrographs of the solids show large cubic domains corresponding to cubic  
10  
11 close packed spherical pores (Figure S2). The absence of any well-defined  $(103)_{\text{hex}}$  reflection in  
12  
13 the XRD patterns, which is expected for the hexagonal close packed array but not for the cubic  
14  
15 stacking, also agree with a major proportion of cubic stacking. Indexing the patterns according to  
16  
17 the cubic ( $Fm\bar{3}m$ ) structure, the unit cell parameter,  $a$ , changes from 81.5 for the extracted  
18  
19 sample, to 70 Å for the sample calcined at 900 °C.  
20  
21  
22  
23  
24



40  
41  
42  
43  
44  
45  
46

**Figure 2:** XRD analysis of SBA-2 samples calcined at different temperatures. The solid black arrow indicates the theoretical position of the  $(103)_{\text{hex}}$  Bragg reflection on the solid calcined at 900°C.

47  
48  
49  
50  
51  
52  
53  
54  
55  
56  
57  
58  
59  
60

The decrease of the  $a$  unit-cell parameter is almost linear with the calcination temperature and represents a 35% volume contraction for the sample calcined at the highest temperature. A summary of these data can be found in Table 2. Evidence on the progressive condensation of the amorphous walls of SBA-2 with increasing temperature has also been found by Ferreiro-Rangel *et al.* using  $^{29}\text{Si}$  MAS-NMR<sup>17</sup>.

**Table 2:** XRD cell parameters for the SBA-2 samples calcined at different temperatures.

Temperature of calcination, °C	a [Å]
solvent-extracted	81.5
700	72.8
800	71.6
900	70.0

The contraction of the unit cell is also clearly evidenced by the experimental isotherms for the adsorption of nitrogen at 77 K (Figure 3). All these isotherms have two clear steps. The first occurs at low pressure and is related to adsorption in the regions of the pore space where the adsorption energy is high – that is, in the channels. The second one, at higher pressure, reflects the filling of the cavities by nitrogen; this filling occurs at higher pressure the larger the cavity. As can be seen in Figure 3, the second step is shifted to lower pressures as we move from the solvent-extracted sample to the three samples calcined at 700, 800 and 900 °C. This shift in the second step indicates a reduction in the mean size of the cavities as the calcination temperature increases, at least up to 700 °C, in broad agreement with the results obtained from the XRD analysis.



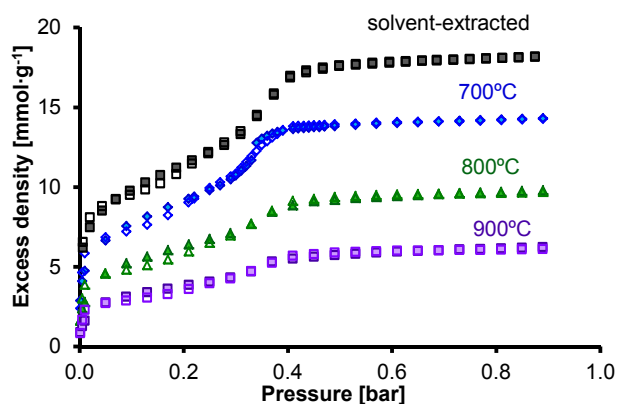


**Figure 3:** Nitrogen adsorption isotherms at 77 K. Full symbols correspond to experimental results while open symbols represent the predictions from simulation.

There is a progressive decrease in nitrogen adsorption as the calcination temperature increases, although the filling of the cavities takes place at the same pressure. This suggests that the size of the cavities accessible to nitrogen in the samples calcined at 700, 800 and 900 °C is approximately the same, while the number of cavities accessible to nitrogen decreases with the calcination temperature. Thus, the combination of the XRD data and nitrogen adsorption isotherms show that, above a calcination temperature of 700 °C, the main effect of the contraction of the framework is to narrow (or perhaps completely close) at least some of the channels, thereby reducing the accessibility of the cavities to nitrogen.

We now go on to quantify the changing pore structure, already evident from the XRD and nitrogen measurements, using the adsorption-percolation analysis presented in Section 3.

The PSD curves for nitrogen adsorption, obtained by analyzing the adsorption data shown in Figure 3, are shown in Figure 4. All the PSDs have two clear maxima: the first is in the microporous region, reflecting adsorption in the channels, and the second is in the mesoporous region, reflecting adsorption in the cavities. These results confirm the conclusions we drew, above, from inspection of the adsorption isotherms themselves.

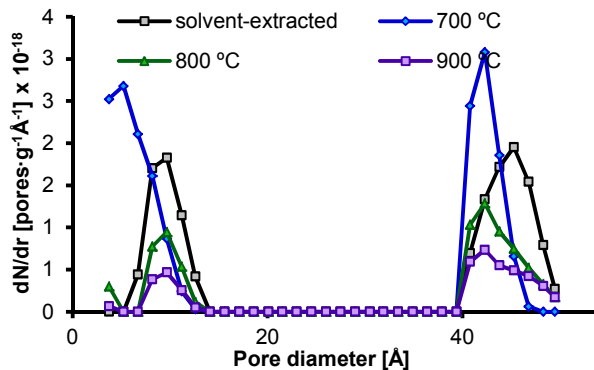


**Figure 4:** PSDs of SBA-2 samples from nitrogen adsorption at 77 K.

Compared with the solvent-extracted sample, the sample calcined at 700 °C shows a marked reduction in both the size of the cavities and the total pore volume. The pore volume accessible to nitrogen decreases further for the samples calcined at 800 and 900 °C while the mean size of the cavities remains constant. This shows that the reduction in the volume accessible to nitrogen for the materials calcined at the higher temperatures is not caused by a reduction in the size of the cavities, but rather in the degree to which the cavities are accessible to nitrogen.

Table 3 shows the results of the adsorption-percolation analysis for the four samples. There is a clear effect of calcination at higher temperatures on the accessibility of the cavities to nitrogen. The solvent-extracted sample is the most highly connected, with a value of the bond occupation probability ( $p^{b,n} = 0.41$ ), and the corresponding effective coordination number ( $z^n = 4.9$ , from Equation 1), that are so big that essentially all the cavities are accessible to nitrogen ( $P^{s,n} = 1.0$ ). At 700 °C, the proportion of the cavities that is accessible to nitrogen is only slightly less than unity;  $P^{s,n} = 0.975$ . Even this relatively small reduction in the accessibility shows that calcination has caused a substantial reduction in the fraction of the channels that are wide enough to accommodate nitrogen molecules,  $p^{b,n}$ , which is reduced to 0.165 at 700 °C, with a corresponding reduction in  $z^n$ . This reflects the form of Figure 1 in which, far from the

percolation threshold, large changes in  $p^{b,n}$  (in adsorption terms, the ability of the channels to accommodate the adsorptive species) correspond to small changes in accessibility; this is characteristic of percolation in general. In contrast, as the percolation threshold is closely approached from above, small changes in  $p^{b,n}$  lead to the collapse of the accessibility, as we will see below.

**Table 3:** Unit cell contraction and percolation parameters for nitrogen adsorption at 77 K.

Cal. Temp [°C]	Cell contraction, %	$P^{s,n}$	$p^{b,n}$	$z^n$
solvent-extracted*	0.0	1.000	0.410	4.90
700	10.7	0.975	0.165	1.98
800	12.1	0.607	0.140	1.68
900	14.1	0.394	0.133	1.59

\* From reference 12

As the calcination temperature is increased to 800 and 900 °C, the connectivity of the network progressively decreases, as shown in Table 3. Nevertheless, even for the least well connected network, that of the sample calcined at 900 °C, the network remains above the percolation threshold for the adsorption of nitrogen; at this temperature,  $p^{b,n} = 0.133$  and  $z^n = 1.59$ , whereas the corresponding figures for the percolation threshold are 0.12 and 1.4 respectively.

The experimental adsorption isotherms at 268 K for C4 and isoC4 are shown in Figure 5 and 6, respectively. The isotherms for both hydrocarbons show a step corresponding to the filling of the cavities, as for the nitrogen isotherms.

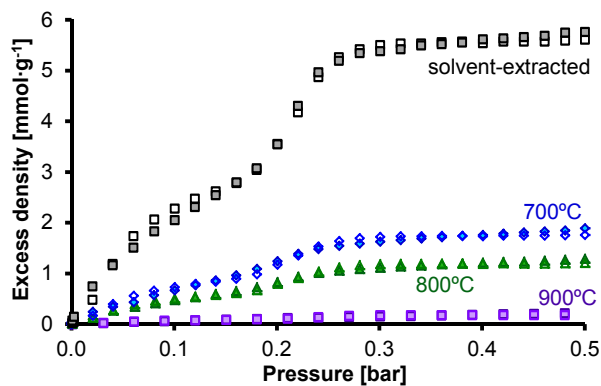


**Figure 5:** C4 adsorption isotherms at 268 K. Full symbols correspond to experimental results while open symbols represent the predictions from simulation.

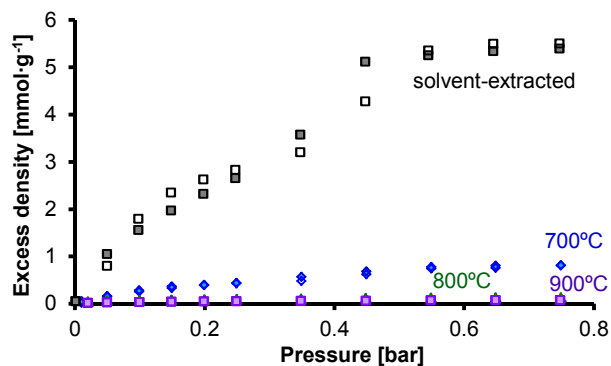


**Figure 6:** IsoC4 adsorption isotherms at 268 K. Full symbols correspond to experimental results while open symbols represent the predictions from simulation.

The step at low pressure which appeared in the nitrogen isotherms is, however, absent; this reflects the fact that the channels have only a small capacity for the adsorption of larger and more complex C4 and isoC4. It is clear that the dramatic decrease in adsorption capacity for both butane isomers on samples calcined at high temperatures, which is more pronounced than in the case of nitrogen adsorption, cannot be attributed solely to the reduction in unit-cell size. The PSDs are shown in Figures 7 and 8. The adsorption-percolation analysis yields the results shown in Table 4.

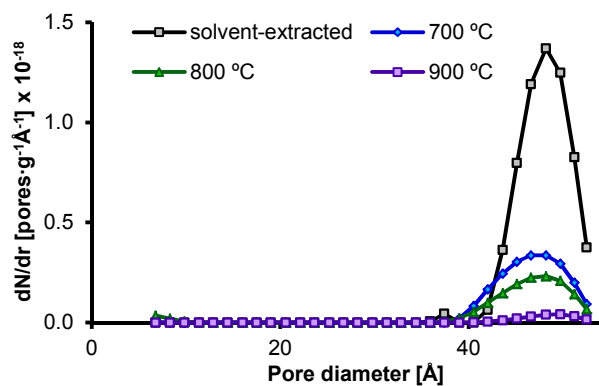


Figure 7: PSDs from C4 adsorption data at 268 K.

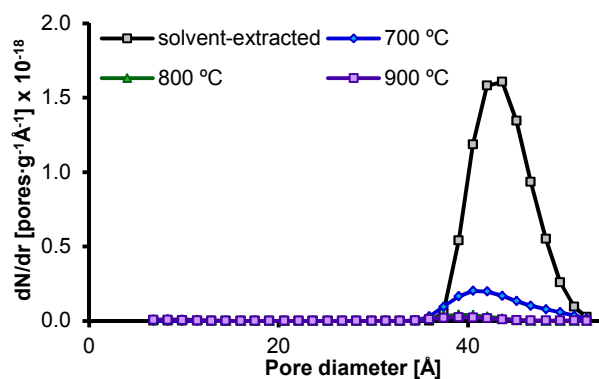


Figure 8: PSDs from isoC4 adsorption data at 268 K.

Table 4: Percolation parameters for butane and isobutane adsorption at 268 K.

Sample	C4			isoC4		
	$P^{s,n}$	$p^{b,C4}$	$z^{C4}$	$P^{s,n}$	$p^{b,isoC4}$	$z^{isoC4}$
Solvent-extracted	0.756	0.147	1.76	0.985	0.170	2.04
700	0.250	0.128	1.54	0.155	0.124	1.49
800	0.168	0.125	1.50	0.023	-	-
900	0.023	-	-	0.015	-	-

\*The absent values indicate that the pore network of the sample is below its percolation threshold so that – beyond noting that point – no connectivity information can be obtained.

1  
2  
3 It is clear that the solvent-extracted sample is freely accessible to both C4 and isoC4, as it is to  
4 nitrogen; the pore structure does not carry out any sieving of the two butane isomers.  
5  
6 Nevertheless, some channels are too small to allow the passage of C4 and isoC4;  $p^b = 0.147$  for  
7  
8 C4 and 0.170 for isoC4, in comparison to 0.410 for nitrogen<sup>18</sup>. [The difference in the values of  
9  
10  $p^b$  for C4 and isoC4 indicates that the isoC4 can pass through slightly more channels than can the  
11  
12 less bulky isomer, C4. While this is, in principle, an anomalous result, the difference is small  
13  
14 compared with the difference between the values of  $p^b$  for the two butane isomers, on the one  
15  
16 hand, and nitrogen, on the other.] As these values for the bond occupation probability are not yet  
17  
18 close to the percolation threshold of the network ( $p^b=0.12$ ), the constrictions in the pore network  
19  
20 do not translate to substantially reduced accessibilities and adsorption capacities. In other words,  
21  
22 despite the much smaller number of channels that are large enough to allow the passage of the  
23  
24 butane isomers, the sub-network formed by these channels is still sufficiently highly connected  
25  
26 to allow access to almost all the cavities.  
27  
28  
29  
30  
31  
32  
33

34 The adsorption-percolation analysis of the samples calcined at higher temperature shows a  
35  
36 very different picture. As in the case of the nitrogen results, shown in Table 3, Table 4 shows  
37  
38 that there is a substantial reduction in the accessibility of the networks at calcination  
39  
40 temperatures of 700 °C and above. This reduction in accessibility, calculated using the  
41  
42 adsorption-percolation analysis, reflects the changes in adsorption shown in the isotherms of  
43  
44 Figures 5 and 6. At a calcination temperature of 700 °C, while adsorption is less than for the  
45  
46 solvent-extracted sample, the adsorption of both isomers remains substantial. The percolation  
47  
48 data of Table 4 confirm that the network of the sample calcined at 700 °C is accessible to both  
49  
50 isomers. At 800 °C, the adsorption of isoC4 is negligible, while there is still substantial (though  
51  
52 much reduced) adsorption of C4. At this temperature, the pore network is accessible to C4 but  
53  
54  
55  
56  
57  
58  
59  
60

1  
2  
3 inaccessible to isoC4. Expressed in percolation terms, the percolation threshold of the network is  
4  
5 passed at different calcination temperatures for the two species. At 800 °C, the network is still  
6  
7 percolating to C4, with 17 % of the cavities accessible and an effective coordination number  
8  
9 ( $z^{b,C4} = 1.5$ ) just above the percolation threshold ( $z^n = 1.4$ ). For isoC4, in contrast, there is very  
10  
11 little adsorption and the pore network is below its percolation threshold. At the still higher  
12  
13 calcination temperature of 900 °C, Table 4 shows that the pore network of the sample is below  
14  
15 the percolation threshold for both butane isomers; the adsorption of both isomers is negligible.  
16  
17 In contrast, as we showed above, the pore network remains accessible to nitrogen even at this  
18  
19 highest calcination temperature.  
20  
21  
22  
23

24 This behavior suggests the possibility of using the calcination process to fine-tune the  
25  
26 accessibility to the SBA-2 mesoporous structure of different adsorptives, in order to achieve a  
27  
28 molecular-sieving effect. For the system we have studied in the present paper, we know that  
29  
30 calcination temperatures above about 700 °C give SBA-2 samples that have a substantial  
31  
32 capacity for the adsorption of pure C4, and a very low capacity for the adsorption of isoC4,  
33  
34 because the latter molecule does not significantly penetrate the pore network. This suggests that,  
35  
36 in adsorption from a mixture of these two species, this material should selectively adsorb C4  
37  
38 over isoC4 – in other words it would exhibit molecular sieving of the branched alkane allowing  
39  
40 the linear alkane to adsorb. The separation of normal and iso-alkanes is an important industrial  
41  
42 adsorption process<sup>28</sup>, and the combination of the high capacity of SBA-2 materials – due to the  
43  
44 cavities – and the tunable molecular sieving – due to the channels – is of potential industrial  
45  
46 interest. More fundamentally, this would be an illustration of the separation manipulation of  
47  
48 pore-size and connectivity effects in the design of porous materials. To test our hypothesis, we  
49  
50 have carried out mixture adsorption experiments with a mixture of C4 and isoC4, using two  
51  
52  
53  
54  
55  
56  
57  
58  
59  
60

1  
2  
3 samples of SBA-2 – one calcined at 550 °C and one at 820 °C. The effectiveness of this  
4  
5 separation can be quantified in terms of the selectivity of the material for C4 over isoC4, defined  
6  
7 as  
8

$$S = \frac{x/(1-x)}{y/(1-y)} \quad (3)$$

9  
10  
11  
12  
13 where  $x$  and  $y$  are the mole fractions of C4 (the more strongly adsorbed species) in the adsorbed  
14  
15 phase and in the bulk-gas phase respectively. Based on our observation that the capacity of SBA-  
16  
17 2 for isoC4 becomes very small at calcination temperatures above about 700 °C, we would  
18  
19 expect the selectivity to be very high for the sample calcined at 820 °C. This is confirmed by the  
20  
21 mixture adsorption measurements, in which we found  $S = 510$  for calcination at 820 °C, and  $S =$   
22  
23 6.6 for calcination at 550 °C. The latter value reflects the adsorption selectivity of the essentially  
24  
25 unconstricted SBA-2 network for C4 over isoC4. It follows, therefore, that the constriction of  
26  
27 the pore network caused by calcination at high temperature, leading to the network becoming  
28  
29 largely inaccessible to isoC4, increases the selectivity by a factor of about 100.  
30  
31  
32  
33  
34  
35  
36

## 37 5. CONCLUSIONS

38  
39 Our study of the adsorption of nitrogen and the two butane isomers on a series of SBA-2  
40  
41 materials calcined at different temperatures gives a clear picture of changes in the pore structure  
42  
43 as the calcination temperature increases. The adsorption-percolation analysis shows that the  
44  
45 network becomes increasingly constricted as the calcination temperature increases, reducing the  
46  
47 accessibility of the network to all three species studied. The more bulky the molecule, the more  
48  
49 susceptible it is to these constrictions. While the SBA-2 pore network remains accessible to  
50  
51 nitrogen even at the highest calcination temperature, 900 °C, it becomes inaccessible to isoC4 at  
52  
53  
54  
55  
56  
57  
58  
59  
60



1  
2  
3 a lower calcination temperature than is the case for C4. The long-range order of SBA-2 remains  
4 intact even at the highest calcination temperature.  
5  
6

7  
8 The fact that the two butane isomers have a different percolation threshold, as a function of the  
9 calcination temperature, suggests using the calcination temperature as a design parameter, the  
10 tuning of which could give an adsorbent with a high selectivity for the C4/isoC4 separation (and,  
11 in principle, for other separations of linear and branched hydrocarbons). Our mixture adsorption  
12 measurements confirmed that this effect occurs in practice. SBA-2 thus demonstrates an  
13 interesting combination of high adsorption capacity, due to the cavities, and a molecular sieving  
14 effect, due to the channels connecting the cavities. Furthermore, it should be possible to  
15 generalize this approach to tune the window size of mesoporous solids containing cages to  
16 optimize molecular selectivity for molecules of sizes extending into the nanometer regime,  
17 where the pores of zeolites – conventionally used for molecular-sieving applications – would be  
18 too small to allow uptake.  
19  
20  
21  
22  
23  
24  
25  
26  
27  
28  
29  
30  
31  
32

### 33 ASSOCIATED CONTENT

34  
35  
36  
37  
38  
39 Nitrogen adsorption isotherms of SBA-2 solvent-extracted and calcined at 550 °C<sup>16</sup> and TEM  
40 micrographs of SBA-2 solid calcined at 900 °C are available as supporting information. This  
41 material is available free of charge via the Internet at <http://pubs.acs.org>.  
42  
43  
44  
45  
46

### 47 AUTHOR INFORMATION

#### 48 Corresponding Author

49  
50  
51 Manuel Pérez-Mendoza. University of Granada. E-mail contact: [mjperezm@ugr.es](mailto:mjperezm@ugr.es)  
52  
53

#### 54 Present Addresses

55  
56  
57  
58  
59  
60

1  
2  
3  
4  
5  
6  
7  
8  
9  
10  
11  
12  
13  
14  
15  
16  
17  
18  
19  
20  
21  
22  
23  
24  
25  
26  
27  
28  
29  
30  
31  
32  
33  
34  
35  
36  
37  
38  
39  
40  
41  
42  
43  
44  
45  
46  
47  
48  
49  
50  
51  
52  
53  
54  
55  
56  
57  
58  
59  
60

✧ Prof. Nigel A. Seaton: Abertay University, Dundee DD1 1HG, United Kingdom.

\* Dr. David Fairen-Jiménez: Department of Chemical Engineering & Biotechnology, University of Cambridge, Pembroke Street, Cambridge, CB2 3RA, UK.

## ACKNOWLEDGMENT

We thank the DeSSANS project (EU FP6 STREP SES6CT2005-020133) and The University of Edinburgh for financial support. J. González also acknowledges financial support from **FRABA-Universidad de Colima** 761/11

## REFERENCES

(1) Kresge, C. T.; Leonowicz, M. E.; Roth, W. J.; Vartuli, J. C.; Beck, J. S. Ordered Mesoporous Molecular-Sieves Synthesized by a Liquid-Crystal Template Mechanism. *Nature* **1992**, *359* (6397), 710-712.

(2) Beck, J. S.; Vartuli, J. C.; Roth, W. J.; Leonowicz, M. E.; Kresge, C. T.; Schmitt, K. D.; Chu, C. T. W.; Olson, D. H.; Sheppard, E. W.; McCullen, S. B., et al. A New Family of Mesoporous Molecular-Sieves Prepared with Liquid-Crystal Templates. *J. Am. Chem. Soc.* **1992**, *114* (27), 10834-10843.

(3) Ciesla, U.; Schuth, F. Ordered Mesoporous Materials. *Microporous Mesoporous Mater.* **1999**, *27* (2-3), 131-149.

(4) Yiu, H. H. P.; Wright, P. A. Enzymes Supported on Ordered Mesoporous Solids: A Special Case of an Inorganic-Organic Hybrid. *J. Mater. Chem.* **2005**, *15* (35-36), 3690-3700.

(5) Garcia-Bennett, A. E. Synthesis, Toxicology and Potential of Ordered Mesoporous Materials in Nanomedicine. *Nanomedicine* **2011**, *6* (5), 867-877.

1  
2  
3 (6) Beck, J. S.; Vartuli, J. C.; Kennedy, G. J.; Kresge, C. T.; Roth, W. J.; Schramm, S. E.  
4  
5 Molecular or Supramolecular Templating - Defining the Role of Surfactant Chemistry in the  
6  
7 Formation of Microporous and Mesoporous Molecular-Sieves. *Chem. Mater.* **1994**, *6* (10), 1816-  
8  
9 1821.  
10

11  
12  
13 (7) Zhao, D. Y.; Huo, Q. S.; Feng, J. L.; Chmelka, B. F.; Stucky, G. D. Nonionic Triblock and  
14  
15 Star Diblock Copolymer and Oligomeric Surfactant Syntheses of Highly Ordered,  
16  
17 Hydrothermally Stable, Mesoporous Silica Structures. *J. Am. Chem. Soc.* **1998**, *120* (24), 6024-  
18  
19 6036.  
20  
21

22  
23  
24 (8) Van der Voort, P.; Mathieu, M.; Mees, F.; Vansant, E. F. Synthesis of High-Quality Mcm-  
25  
26 48 and Mcm-41 by Means of the Gemini Surfactant Method. *J. Phys. Chem. B* **1998**, *102* (44),  
27  
28 8847-8851.  
29

30  
31  
32 (9) Tanev, P. T.; Pinnavaia, T. J. A Neutral Templating Route to Mesoporous Molecular-  
33  
34 Sieves. *Science* **1995**, *267* (5199), 865-867.  
35

36  
37  
38 (10) Park, S. S.; Ha, C. S. Organic-Inorganic Hybrid Mesoporous Silicas: Functionalization,  
39  
40 Pore Size, and Morphology Control. *Chemical Record* **2006**, *6* (1), 32-42.  
41

42  
43 (11) Angloher, S.; Bein, T., *Organic Functionalisation of Mesoporous Silica*. ELSEVIER  
44  
45 SCIENCE BV: AMSTERDAM, 2005; p 2017-2026.  
46  
47

48  
49 (12) Hunter, H. M. A.; Garcia-Bennett, A. E.; Shannon, I. J.; Zhou, W. Z.; Wright, P. A.  
50  
51 Particle Morphology and Microstructure in the Mesoporous Silicate Sba-2. *J. Mater. Chem.*  
52  
53 **2002**, *12* (1), 20-23.  
54  
55

1  
2  
3 (13) Zhou, W. Z.; Hunter, H. M. A.; Wright, P. A.; Ge, Q. F.; Thomas, J. M. Imaging the Pore  
4 Structure and Polytypic Intergrowths in Mesoporous Silica. *J. Phys. Chem. B* **1998**, *102* (36),  
5 6933-6936.  
6  
7

8  
9  
10 (14) Perez-Mendoza, M.; Gonzalez, J.; Wright, P. A.; Seaton, N. A. Elucidation of the Pore  
11 Structure of Sba-2 Using Monte Carlo Simulation to Interpret Experimental Data for the  
12 Adsorption of Light Hydrocarbons. *Langmuir* **2004**, *20* (18), 7653-7658.  
13  
14  
15

16 (15) Han, L.; Sakamoto, Y.; Terasaki, O.; Li, Y.; Che, S. Synthesis of Carboxylic Group  
17 Functionalized Mesoporous Silicas (Cfmss) with Various Structures. *J. Mater. Chem.* **2007**, *17*  
18 (12), 1216-1221.  
19  
20  
21  
22  
23  
24

25 (16) Ma, Y. H.; Han, L.; Miyasaka, K.; Oleynikov, P.; Che, S. N.; Terasaki, O. Structural  
26 Study of Hexagonal Close-Packed Silica Mesoporous Crystal. *Chem. Mater.* **2013**, *25* (10),  
27 2184-2191.  
28  
29  
30  
31  
32

33 (17) Ferreiro-Rangel, C. A.; Lozinska, M. M.; Wright, P. A.; Seaton, N. A.; Duren, T. Kinetic  
34 Monte Carlo Simulation of the Synthesis of Periodic Mesoporous Silicas Sba-2 and Stac-1:  
35 Generation of Realistic Atomistic Models. *J. Phys. Chem. C* **2012**, *116* (39), 20966-20974.  
36  
37  
38  
39  
40  
41

42 (18) Perez-Mendoza, M.; Gonzalez, J.; Wright, P. A.; Seaton, N. A. Structure of the  
43 Mesoporous Silica SBA-2, Determined by a Percolation Analysis of Adsorption. *Langmuir* **2004**,  
44 *20* (22), 9856-9860.  
45  
46  
47  
48  
49

50 (19) Yanuka, M. Percolation Theory and Capilarity in Relation to Pore Geometry. University  
51 of Guelph, 1984.  
52  
53  
54  
55  
56  
57  
58  
59  
60

1  
2  
3 (20) Yun, J. H.; Duren, T.; Keil, F. J.; Seaton, N. A. Adsorption of Methane, Ethane, and Their  
4 Binary Mixtures on Mcm-41: Experimental Evaluation of Methods for the Prediction of  
5 Adsorption Equilibrium. *Langmuir* **2002**, *18* (7), 2693-2701.  
6  
7

8  
9  
10  
11 (21) Kjems, J. K.; Dolling, G. Crystal Dynamics of Nitrogen - Cubic Alpha-Phase. *Phys. Rev.*  
12 *B* **1975**, *11* (4), 1639-1647.  
13  
14

15  
16  
17 (22) Bezus, A. G.; Kiselev, A. V.; Lopatkin, A. A.; Du, P. Q. Molecular Statistical Calculation  
18 of Thermodynamic Adsorption Characteristics of Zeolites Using Atom-Atom Approximation .1.  
19 Adsorption of Methane by Zeolite Nax. *J. Chem. Soc. Faraday Trans.* **1978**, *74*, 367-379.  
20  
21

22  
23  
24 (23) Jorgensen, W. L.; Madura, J. D.; Swenson, C. J. Optimized Intermolecular Potential  
25 Functions for Liquid Hydrocarbons. *J. Am. Chem. Soc.* **1984**, *106* (22), 6638-6646.  
26  
27

28  
29  
30 (24) Lorenz, C. D.; May, R.; Ziff, R. M. Similarity of Percolation Thresholds on the Hcp and  
31 Fcc Lattices. *J. Stat. Phys.* **2000**, *98* (3-4), 961-970.  
32  
33

34  
35  
36 (25) Davies, G. M.; Seaton, N. A.; Vassiliadis, V. S. Calculation of Pore Size Distributions of  
37 Activated Carbons from Adsorption Isotherms. *Langmuir* **1999**, *15* (23), 8235-8245.  
38  
39

40  
41 (26) Gonzalez, J. PhD Thesis University of St. Andrews, 2005.  
42  
43

44  
45 (27) Huo, Q. S.; Leon, R.; Petroff, P. M.; Stucky, G. D. Mesostucture Design with Gemini  
46 Surfactants - Supercage Formation in a 3-Dimensional Hexagonal Array. *Science* **1995**, *268*  
47 (5215), 1324-1327.  
48  
49

50  
51 (28) Yang, R. T., *Gas Separation by Adsorption Processes*. Imperial College Press: 1987.  
52  
53  
54  
55  
56  
57  
58  
59  
60

## TABLE OF CONTENTS

